

Electro-Optic Measurements of PbS, PbSe, and PbTe†

D. E. ASPNES* AND M. CARDONA‡

Department of Physics, Brown University, Providence, Rhode Island 02912

(Received 5 January 1968)

The band structures of the lead salts PbS, PbSe, and PbTe have been studied by electro-optic methods. Electroabsorption and electroreflectance measurements have been made over the energy ranges 0.25 to 0.65 eV and 0.6 to 5.5 eV, respectively, using an electrolyte to produce electric fields at the surface of these materials. An enhancement of the existing structure in absorption and reflection was generally observed, together with new structure apparently not related to formerly observed transitions. The analysis of these structures leads to the symmetry and energy of several transitions not previously seen. The experimental results are correlated with the band-structure calculations of Lin and Kleinman, and in general support their results.

I. INTRODUCTION

THE lead salts PbS, PbSe, and PbTe form an important group of semiconducting compounds. Crystallizing in the rocksalt structure, these IV-VI compounds are characterized by low-energy gaps and large static dielectric constants. The natural abundance of PbS made it one of the first semiconducting compounds to be studied. As a result of this, of the relative ease with which PbSe and PbTe single crystals could be prepared, and of the development of methods of growing single-crystal epitaxial films of all three compounds,^{1,2} much information about their band properties has been obtained by means of electrical,³⁻⁶ optical,^{4,7-10} magneto-optical,¹¹⁻¹³ cyclotronresonance,¹⁴⁻¹⁶ re-

combination radiation,¹⁷ pressure measurements,¹⁸⁻²⁰ and photoemission studies.²¹ This mass of data has stimulated band-structure calculations which are now available in the literature.^{22,23} Based on the above measurements which give energy band parameters near the fundamental absorption edges and on reflectivity measurements for higher-lying transitions,⁷ these calculations give a fairly extensive picture of the energy band structure of these materials. The present work was undertaken with the objective of testing the band-structure calculations by utilizing the electroabsorption and electroreflectance techniques recently developed and explored theoretically²⁴⁻²⁷ and experimentally.²⁸⁻³⁴

† Supported by the U. S. Army Research Office (Durham) and the National Science Foundation.

* Present address: Bell Telephone Laboratories, Murray Hill, N. J. 07974.

‡ Alfred P. Sloan Research Fellow.

¹ R. B. Schoolar and J. N. Zemel, *J. Appl. Phys.* **35**, 1848 (1964).

² J. N. Zemel, J. D. Jensen, and R. B. Schoolar, *Phys. Rev.* **140**, A330 (1965).

³ W. W. Scanlon, in *Solid State Physics*, edited by F. Seitz and D. Turnbull (Academic Press Inc., New York, 1959), Vol. 9, p. 83.

⁴ R. N. Tauber, A. A. Machonis, and I. B. Cadoff, *J. Appl. Phys.* **37**, 4855 (1966).

⁵ A. A. Andreev and V. N. Radionov, *Fiz. Tekhn. Pol.* **1**, 183 (1967) [English transl.: *Soviet Phys.—Semicond.* **1**, 145 (1967)].

⁶ Yu. V. Mal'tsev, E. D. Nesberg, A. V. Petrov, S. A. Semiletov, and Yu. I. Ukhanov, *Fiz. Tverd. Tela* **8**, 2154 (1966) [English transl.: *Soviet Phys.—Solid State* **8**, 1713 (1967)].

⁷ M. Cardona and D. L. Greenaway, *Phys. Rev.* **133**, A1685 (1964).

⁸ M. Cardona, *J. Appl. Phys.* **36**, 2181 (1965).

⁹ R. B. Schoolar and J. R. Dixon, *Phys. Rev.* **137**, A667 (1965).

¹⁰ P. R. Wessel, *Phys. Rev.* **153**, 826 (1967).

¹¹ E. D. Palik, D. L. Mitchell, and J. N. Zemel, *Phys. Rev.* **135**, A763 (1966).

¹² D. L. Mitchell, E. D. Palik, and J. N. Zemel, in *Proceedings of the Seventh International Conference on the Physics of Semiconductors, Paris, 1964* (Academic Press Inc., New York, 1965), Vol. I, p. 325; D. L. Mitchell, E. D. Palik, and R. F. Wallis, *Phys. Rev. Letters* **14**, 827 (1965).

¹³ D. L. Mitchell, E. D. Palik, and J. N. Zemel, in *Proceedings of the International Conference on the Physics of Semiconductors* (The Physical Society of Japan, Tokyo, 1966), p. 197.

¹⁴ P. J. Stiles, E. Burstein, and K. N. Langenberg, in *Proceedings of the International Conference on the Physics of Semiconductors, Exeter, 1962* (The Institute of Physics and the Physical Society, London, 1962), p. 577.

¹⁵ R. Nii, *J. Phys. Soc. Japan* **19**, 58 (1964).

¹⁶ S. Bermon, *Phys. Rev.* **158**, 723 (1967).

¹⁷ G. F. K. Garlick, in *Proceedings of the Seventh International Conference on the Physics of Semiconductors, Paris, 1964* (Academic Press Inc., New York, 1965), Vol. IV, p. 3; E. R. Washwell and K. F. Cuff, *ibid.*, p. 12.

¹⁸ W. Paul, M. Demeis, and L. X. Finegold, in *Proceedings of the International Conference on the Physics of Semiconductors, Exeter 1962* (The Institute of Physics and the Physical Society, London 1962), p. 712.

¹⁹ A. A. Averkin, U. V. Ilisavsky, and A. R. Regel, in *Proceedings of the International Conference on the Physics of Semiconductors, Exeter, 1962* (The Institute of Physics and the Physical Society, London, 1962), p. 690.

²⁰ J. M. Besson, J. F. Butler, A. R. Calawa, W. Paul, and R. H. Rediker, *Appl. Phys. Letters* **7**, 206 (1965).

²¹ W. E. Spicer and G. J. Lapeyre, *Phys. Rev.* **139**, A565 (1965).

²² P. J. Lin and L. Kleinman, *Phys. Rev.* **142**, 478 (1966).

²³ D. L. Mitchell and R. F. Wallis, *Phys. Rev.* **151**, 581 (1966).

²⁴ W. Franz, *Z. Naturforsch.* **13**, 484 (1958); L. V. Keldysh, *Zh. Eksperim. i Teor. Fiz.* **34**, 1138 (1958) [English transl.: *Soviet Phys.—JETP* **7**, 788 (1958)].

²⁵ J. C. Phillips and B. O. Seraphin, *Phys. Rev. Letters* **15**, 107 (1965); J. C. Phillips, *Phys. Rev.* **146**, 584 (1966).

²⁶ F. Aymerich and F. Bassani, *Nuovo Cimento* **48**, 358 (1967).

²⁷ D. E. Aspnes, *Phys. Rev.* **147**, 554 (1966); **153**, 972 (1967).

²⁸ B. O. Seraphin and R. B. Hess, *Phys. Rev. Letters* **14**, 138 (1965); B. O. Seraphin and N. Bottka, *Phys. Rev.* **145**, 628 (1966).

²⁹ K. L. Shaklee, F. H. Pollak, and M. Cardona, *Phys. Rev. Letters* **15**, 883 (1965).

³⁰ M. Cardona, K. L. Shaklee, and F. H. Pollak, in *Proceedings of the International Conference on the Physics of Semiconductors* (The Physical Society of Japan, Tokyo, 1966), p. 89.

³¹ M. Cardona, K. L. Shaklee, and F. H. Pollak, *Phys. Rev.* **154**, 696 (1967).

³² A. Frova, P. Handler, F. A. Germano, and D. E. Aspnes, *Phys. Rev.* **145**, 575 (1966).

³³ V. Rehn and D. S. Keyser, *Phys. Rev. Letters* **18**, 848 (1967).

³⁴ R. A. Forman and M. Cardona, in *Proceedings of the International Conference on II-VI Semiconducting Compounds, 1967, Brown University*, edited by D. G. Thomas (W. A. Benjamin, Inc., New York, 1967).

Electro-optic measurements enhance the structure normally seen in reflectance or absorption and can, in principle, distinguish among the various types of critical points. Using these methods, it should be possible to obtain a better experimental picture of the energy band structure of these materials at energies above the fundamental threshold.

A description of the experimental techniques and theoretical background is given in Sec. II, followed by a presentation and discussion of results in Sec. III.

II. EXPERIMENTAL

The electrolyte method^{29,31} was used for the electro-optic measurements because of the relatively high conductivity resulting from the small forbidden gaps of these materials. The electric field is obtained at the surface of the semiconductor in the blocking direction of polarity by the generation of a space-charge region adjacent to the surface. The transverse electric field method, which has been used with success in other semiconductors,³³⁻³⁵ cannot be used because of the high conductivity of these compounds even in the intrinsic condition.

With the exception of one natural crystal of PbS, all measurements were performed on epitaxially deposited films which were made by the method of Scholar and Zemel.¹ NaCl was primarily used as the substrate material, but measurements were also made on PbSe and PbTe using mica as a substrate. Silicon was also used with some success. It is known that the cubic semiconductors orient in the [100] direction on cleaved faces of NaCl¹; the probable orientation on mica is [111].³⁶ The thickness of all epitaxial layers was measured by means of a quartz crystal oscillator thickness monitor.³⁷ Electrical-resistivity and Hall-effect measurements were done using the van der Pauw³⁸ technique, with four probes on the rectangular crystals.

Several films of *n*-type PbS, which was the type obtained after evaporation, were doped by heating to 350°C for $\frac{1}{2}$ h in an evacuated Pyrex tube containing sulfur at the partial pressure of room temperature, achieved by keeping one end of the tube at room temperature. By this method, *p*-type PbS films of resistivity of the order of 10^{18} cm⁻³ were obtained. Since the spectra of the two types were nearly identical, no attempt was made to control the carrier concentrations or types for PbSe or PbTe. The measured samples of these materials were *p* type.

Electrical contact to the epitaxial films and to the natural PbS crystal was made with silver paint along

³⁵ R. A. Forman, D. E. Aspnes, and M. Cardona (to be published).

³⁶ D. W. Pashley [Phil. Mag. (London) 8, 316] observes a (111) orientation of the cubic semiconductors SnAs and SnTe on mica for very thin depositions (1 nm).

³⁷ Manufactured by Edwards High Vacuum, Inc., Grand Island, N. Y.

³⁸ L. van der Pauw, Philips Res. Rept. 13, 1 (1958).

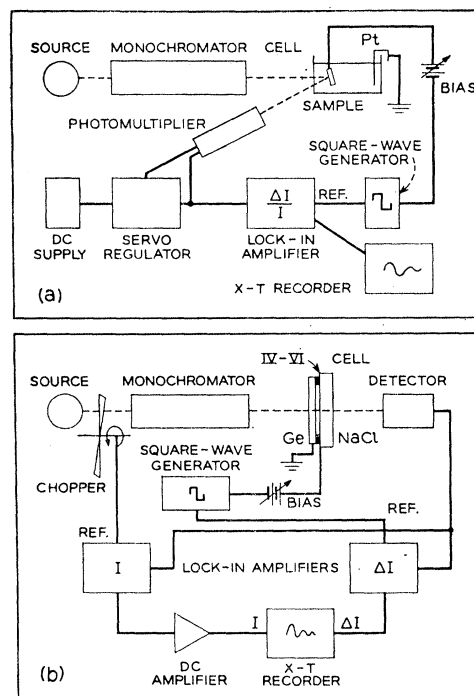


FIG. 1. Experimental apparatus. (a) Photomultiplier detector in electroreflectance; (b) solid-state detector in electroabsorption.

one edge. A platinum strip was used to obtain contact to the electrolyte in a cell for electro-reflectance measurements. For electroabsorption measurements near the fundamental edges involved, where the electrolyte absorbs, a thin film of electrolyte was used as a capillary layer between the sample and a conducting (10- Ω cm) germanium window, separated by a 0.25-mil Mylar spacer with a window in it.³⁹ The contact to the electrolyte in the transmission configuration was made through the conducting germanium window. Because of the high solubility of the substrate NaCl in the common polar electrolytes, the organic electrolyte propylene carbonate, with tetrabutyl ammonium perchlorate as a solute, was used for all measurements and gave satisfactory results.⁴⁰

The standard phase-sensitive detection methods were employed to measure the change in reflected or absorbed light intensity caused by the applied electric field which varied periodically in time. Figure 1 shows a block diagram of the apparatus used. A square-wave voltage at 100 Hz added to an adjustable dc bias was used to drive the sample with respect to the grounded electrolyte contact in order to produce the electric field. The infrared optical system for electroabsorption measurements consisted of a Globar source, a Bausch and Lomb 0.5-m monochromator with a 150-line/mm

³⁹ F. Lukeš and E. Schmidt, Phys. Letters 23, 413 (1966).

⁴⁰ Propylene carbonate supplied by Eastman Kodak Co., Rochester, N. Y.; tetrabutyl ammonium perchlorate by G. Frederick Smith Chemical Co., Columbus, Ohio.

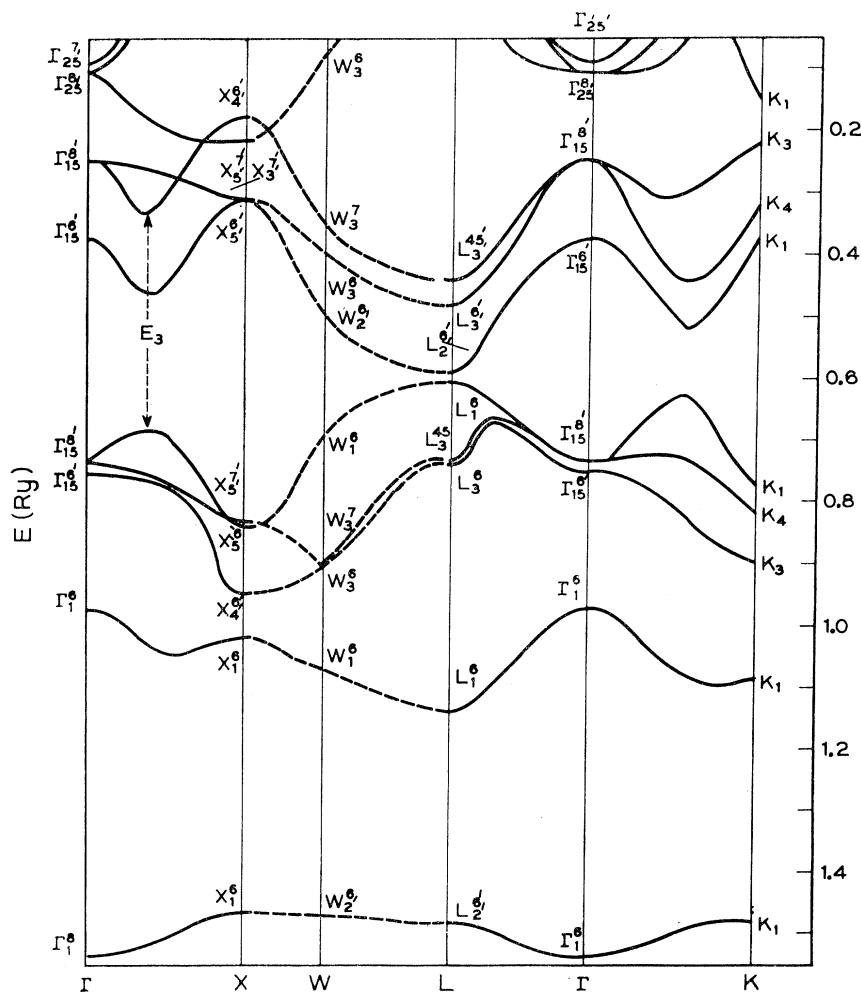


FIG. 2. The energy band structure of PbS, calculated by Lin and Kleinman (Ref. 22).

grating blazed at 2μ , and a PbSe detector for measurements in the region of 1.6 to 5μ . By cooling the detector, the wavelength range of the system could in principle be extended to about 5.8μ , although CO_2 absorption in air resulted in extremely low light levels beyond 5μ . The 150-Hz intensity I and the 100-Hz change of intensity ΔI signals were phase-sensitively detected by Princeton Applied Research Model JB-6 and HR-8 lock-in amplifiers, respectively, and the ratio $\Delta I/I$ obtained directly on the recorder as described elsewhere.⁴¹ The same system with a SunGun source, a 300-line/mm grating blazed at 2μ , and a PbS detector was used for electroreflectance measurements from the propylene carbonate cutoff at 2μ to about 0.6μ (2 eV). From 800 to 200 nm (6 eV), a Spex Model 1700-II grating monochromator with either a 600-line/mm grating blazed at 500 nm or a 1200-line/mm grating blazed at 200 nm was used with a high-pressure Osram xenon arc, quartz optics, and a Dumont 6911 phototube with S-1 response for the visible region or an EMI 6256B phototube with S-13 response for uv work. The

⁴¹ D. E. Aspnes, Rev. Sci. Instr. 38, 1663 (1967).

ratio $\Delta I/I$ was obtained in the usual manner by controlling the photomultiplier voltage by means of a feedback servo system which kept the dc current through the phototube constant.³¹

Because thin films and a high-resistivity electrolyte were used, fairly large phase lags were observed between the fundamentals of the driving voltage and the resultant change of intensity ΔI . This is attributable to RC time lags caused by the large space-charge region capacitance in PbS, PbSe, and PbTe, caused by their very large dielectric constants.⁴² In order to determine the correct phase lag, zero relative phase shift was obtained by decreasing the frequency (at the expense of the signal-to-noise ratio) until the observed phase of the fundamental of ΔI was approximately equal to the phase of the fundamental of the driving voltage. This generally occurred around 10 Hz . The signal-to-noise ratio was best at 100 Hz , after which

⁴² The dielectric constants of PbS, PbSe, and PbTe are not known very accurately but appear to be around 400. On the basis of long-wavelength optical mode propagation, a value of 397 ± 30 for PbTe was obtained by E. G. Bylander and M. Haas, Solid State Commun. 4, 51 (1966). See also references therein.

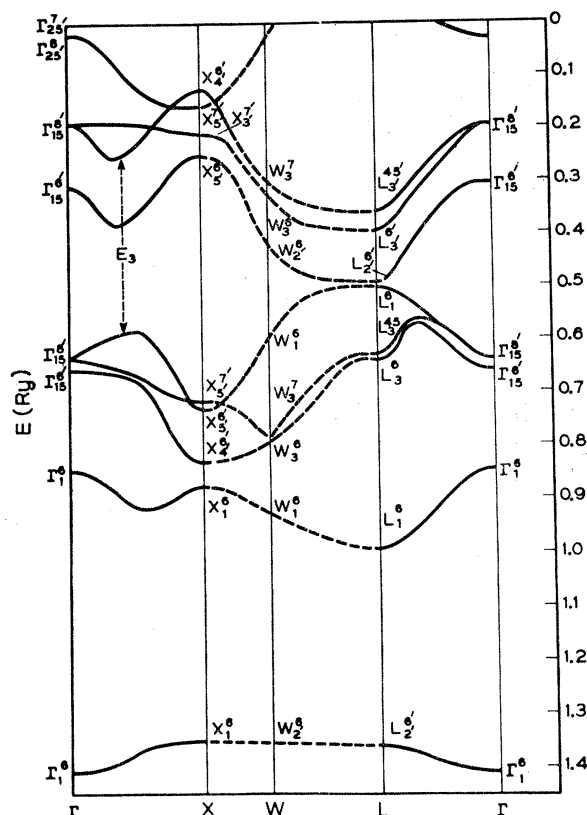
TABLE I. Critical-point energies and symmetries for PbS, PbSe, and PbTe along high-symmetry directions, from the band-structure calculations of Lin and Kleinman.^a Critical-point types are the most probable assuming uniform variation of E and \hbar in directions perpendicular to the high-symmetry axes. Assignment of reflectivity peaks is that of Lin and Kleinman. Uncertainty in the energies listed is taken to be ± 0.4 eV.

Transition	Peak	Type	PbS	PbSe	PbTe
$L_1^6(2) \rightarrow L_2^{6'}(2)$	$E_0, {}^b E_1^c$	M_0	0.25 eV	0.11 eV	1.30 eV
$\Sigma_1^5(3) \rightarrow \Sigma_1^5(4)$		M_1	1.48 eV	...	1.62 eV
$L_1^6(2) \rightarrow L_3^{6'}(1)$	$E_1, {}^b E_0^c$	M_0	1.72 eV	1.48 eV	0.21 eV
$L_3^{45}(1) \rightarrow L_2^{6'}(2)$		M_0+M_1	1.92 eV	1.85 eV	2.06 eV
$L_3^6(1) \rightarrow L_2^{6'}(2)$	E_2^c	M_0+M_1	2.00 eV	2.00 eV	2.50 eV
$L_1^6(2) \rightarrow L_3^{45'}(1)$		M_0	2.25 eV	2.00 eV	1.46 eV
$\Sigma_1^5(3) \rightarrow \Sigma_4^5(2)$		M_1	2.52 eV	...	1.15 eV
$\Sigma_1^5(1) \rightarrow \Sigma_1^5(4)$		M_1	2.85 eV	...	2.60 eV
$\Delta^6(4) \rightarrow \Delta^6(5)$		M_2	3.02 eV	2.81 eV	1.80 eV
$L_3^{45}(1) \rightarrow L_3^6(1)$		M_0+M_1	3.37 eV	3.19 eV	0.98 eV
$L_3^6(1) \rightarrow L_3^{6'}(1)$	E_2^b	M_0+M_1	3.45 eV	3.34 eV	1.41 eV
$\Sigma_3^5(1) \rightarrow \Sigma_1^5(4)$		M_1	3.84 eV	...	3.90 eV
$\Sigma_4^5(1) \rightarrow \Sigma_4^5(2)$		M_1	3.89 eV	...	1.95 eV
$L_3^{45}(1) \rightarrow L_3^{45'}(1)$		M_0+M_1	3.94 eV	3.68 eV	2.21 eV
$\Delta^7(1) \rightarrow \Delta^6(5)$		M_2	3.98 eV	3.75 eV	2.58 eV
$L_3^6(1) \rightarrow L_3^{45'}(1)$		M_0+M_1	4.02 eV	3.83 eV	2.65 eV
$\Delta^6(3) \rightarrow \Delta^6(5)$		M_2	4.14 eV	3.89 eV	3.08 eV
$\Delta^6(4) \rightarrow \Delta^6(6)$	E_3^c	M_2	4.43 eV	4.62 eV	3.36 eV
$\Sigma_1^5(3) \rightarrow \Sigma_3^5(2)$		M_1	4.45 eV	...	3.36 eV
$\Delta^7(1) \rightarrow \Delta^6(6)$		M_2	5.75 eV	5.49 eV	4.08 eV

^a Reference 22.
^b PbS, PbSe.
^c PbTe.

the signal decreased rapidly with increasing frequency. 100 Hz was chosen as the optimum frequency at which to run, in spite of the relatively large phase shifts which meant that the internal electric field as a function of time was considerably distorted from the square wave of the applied voltage. Because of this distortion of the electric-field waveform, no attempt was made to fit the shape of the electro-optic measurements to the electro-optic functions, since the time variation of the field, even if it were known, would lead to a complicated time average in calculating $\Delta R/R$ or $\Delta\alpha$ so that the detailed shape of the electro-optic functions²⁷ $F(\eta)$ and $G(\eta)$ would not be obtained.

In addition to signal averaging due to the distorted waveform, there exists the problem of the slow buildup of the polarization layer at the electrolyte-semiconductor interface, which usually took about 5 min and results in an effective change of dc biasing conditions during a measurement run. Measurements were taken after equilibrium was reached in most cases, although this was not completely necessary since the interpretation of the results is limited to location and general shape of structure in the electro-optic spectrum, which is practically independent of this effect. The rough experimental shape and sign of ΔI were reproducible among runs and represent valid information upon which to base the analysis.



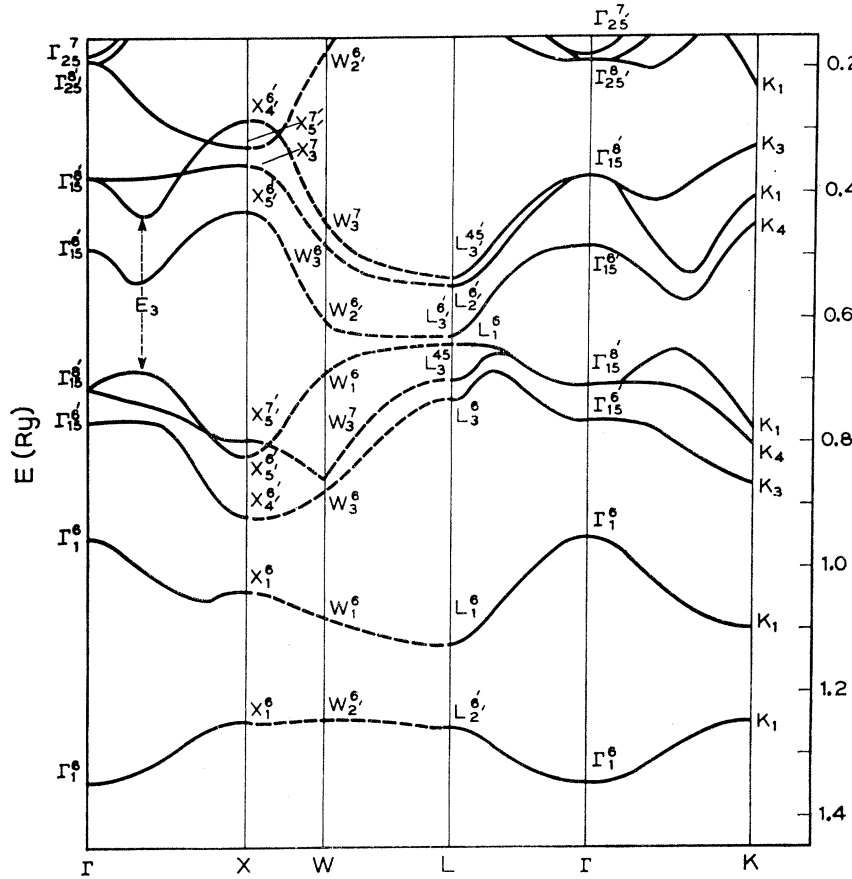


FIG. 4. The energy band structure of PbTe, calculated by Lin and Kleinman (Ref. 22).

higher energies.⁴³ Although the Σ direction bands are not available for PbSe, we assume that they will closely resemble those of PbS in accordance with the rest of the band structure.

The reflectivity spectra of PbS, PbSe, and PbTe as measured by Cardona and Greenaway⁷ are reproduced in Fig. 5. The dominant structures of each spectrum have been labeled E_1 , the first shoulder, E_2 , the highest peak of the reflectivity spectrum, and E_3 , a high-energy shoulder on the main peak. Higher structure will not concern us in this paper. The lowest edges E_0 are below the region of the measurements of Fig. 5.

The structure in an electroreflectance spectrum is related in a rather complicated fashion to structure in the real and imaginary parts of the dielectric constant ϵ_1 and ϵ_2 in the presence of an electric field. Since the parameters obtained from the microscopic theory are ϵ_1 and ϵ_2 , some processing of the electroreflectance data is necessary before comparing them with theoretical predictions. One possible approach is to obtain $\Delta\epsilon_1$ and

$\Delta\epsilon_2$ from the electroreflectance spectrum by using the Kramers-Kronig relations.³¹ Another approach²⁸ involves the evaluation of the individual contribution of $\Delta\epsilon_1$ and $\Delta\epsilon_2$ to the electroreflectance $\Delta R/R$ and the evaluation of the possible line shapes for $\Delta R/R$ from the theoretical shapes of $\Delta\epsilon_1$ and $\Delta\epsilon_2$. We follow this

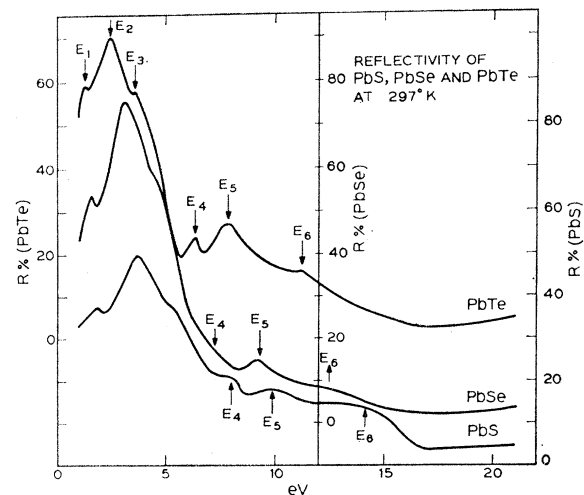


Fig. 5. Reflectivity of PbS, PbSe, and PbTe in the energy range to 25 eV, measured by Cardona and Greenaway (Ref. 7).

⁴³ Lin and Kleinman discuss the accuracy of their band-structure calculations but put no limit on it. The determination of the critical-point energy by measurement of the separation of the energy band diagrams is an additional source of error, since it will be noted that the energies obtained in this way are somewhat different from those given in Table V of Ref. 22 for corresponding transitions. In the interest of consistency, all energy differences in Table I are determined graphically.

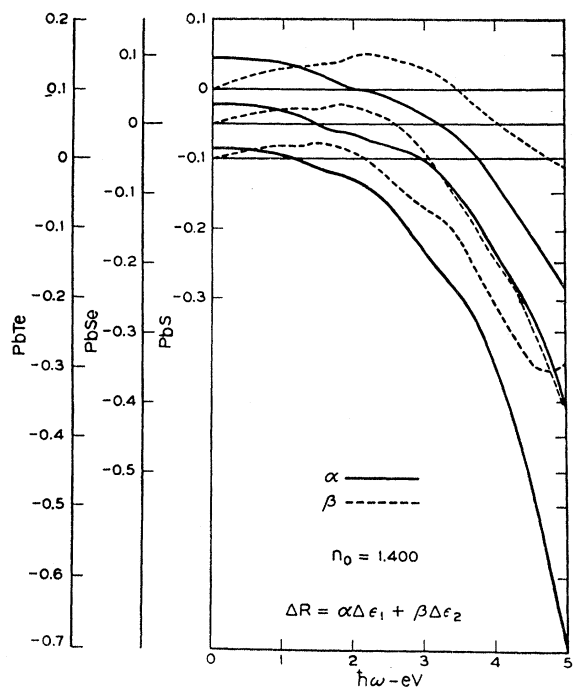


FIG. 6. The coefficients $\alpha(n,k)$ and $\beta(n,k)$ for PbS, PbSe, and PbTe in contact with a liquid of index of refraction $n_0=1.400$, calculated from the values of n and k of Cardona and Greenaway (Ref. 7). Note displaced ordinates among these compounds.

last approach:

$$\Delta R/R = \alpha(n,k)\Delta\epsilon_1 + \beta(n,k)\Delta\epsilon_2. \quad (1)$$

The coefficients α and β are obtained by differentiating the Fresnel reflection formula for normal incidence.²⁸ We have calculated α and β from the values of n and k obtained by Cardona and Greenaway⁷ and the results are given in Fig. 6 for PbS, PbSe, and PbTe in contact with a liquid of index of refraction $n=1.400$. For electroabsorption, only the change in ϵ_2 is significant if, as was true in our experiments, the absorption by the sample is much larger than the loss by reflection. In order to facilitate the analysis, we show in Fig. 7 the changes of the real and imaginary parts of the dielectric constant with field, defined by $\Delta\epsilon = \epsilon(\mathcal{E}) - \epsilon(0)$, for all six possible cases²⁷ (M_0 , M_1 and M_2 transverse and parallel, and M_3). A broadening of $\Gamma = \frac{1}{2}\hbar\theta$ (see Ref. 27) has been assumed to provide a more realistic fit between theory and experiment.

IV. RESULTS AND DISCUSSION

A. PbS and PbSe

Because of the similarity between PbS and PbSe, these will be discussed together and PbTe will be treated separately in Sec. IV B. We consider first electroabsorption results obtained with an epitaxial film of PbS on an NaCl single-crystal substrate. This PbS epitaxial film, of thickness 0.6μ as measured by

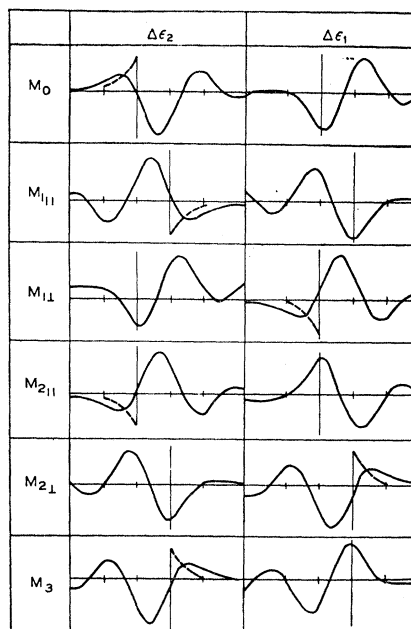


FIG. 7. Theoretical changes of the real ($\Delta\epsilon_1$) and imaginary ($\Delta\epsilon_2$) parts of the dielectric constant in an applied electric field for the six different cases of critical points in an arbitrarily oriented electric field. A broadening $\Gamma = \frac{1}{2}\hbar\theta$ has been assumed in the solid curves; the dashed portions show the functions $F(\eta)$ for zero broadening. Energy increases to the right. Abscissa units are $\hbar\theta$ and the ordinate is placed at the threshold energy.

the quartz crystal monitor during evaporation, was n type with $n=2 \times 10^{18} \text{ cm}^{-3}$, $\rho=0.020 \Omega \text{ cm}$, and $\mu_H=100 \text{ cm}^2 \text{ V}^{-1} \text{ sec}^{-1}$ as determined by a van der Pauw³⁸ measurement. The experimental electroabsorption configuration was that of the conducting Ge window with a thin electrolyte film. A 100-Hz square-wave voltage with series dc bias was applied to the PbS layer with the Ge window grounded. A square wave plus dc bias is describable by two voltages which represent the extremes of the wave, and these two voltages of the PbS layer with respect to the Ge window are given on the figures which follow. In every case we use the convention that a positive value of $\Delta I/I$ means that the fundamental Fourier components of both $\Delta I/I$ (and therefore $+\Delta R$ and $-\Delta\alpha$) and the voltage applied to the sample are in phase (after compensating for any phase lags in the system which are determined by measuring the limiting phase as the frequency approaches zero).

Figure 8 shows the electroabsorption results of the PbS layer for two values of dc bias added to a constant amplitude square wave. $\Delta I/I$, proportional to $-\Delta\alpha$, is plotted as a function of energy. The low-energy limit is determined by the detector and the light intensity, the upper limit by the cutoff of the Ge window. The two curves of Fig. 8 are very nearly mirror images, indicating that it is possible to obtain a maximum field of either sign for the appropriate bias polarity, that is, one can go from zero field to a field

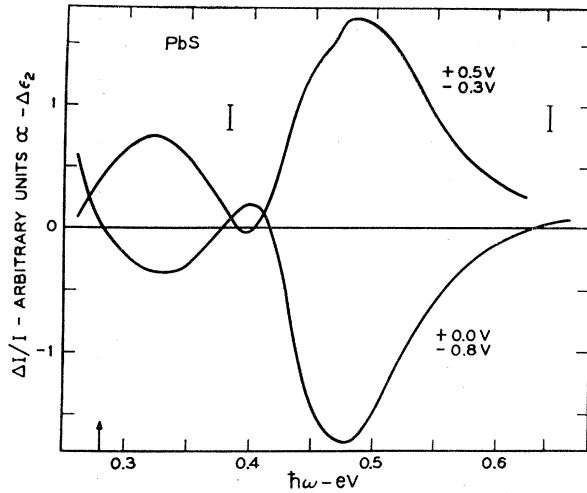


FIG. 8. Electroabsorption of nominal $0.6\text{-}\mu$ n -type epitaxial PbS film on NaCl substrate. Units of $\Delta I/I$ are arbitrary but of the order of 10^{-4} . Uncertainties are indicated as bars in figure. Arrow locates energy of measured first transmission interference maximum in film. Voltages shown are the limits of square wave plus series dc bias.

directed either into or out of the PbS film simply by changing the dc bias. The 180° phase shift is apparent and results because the interface and electro-optic effects depend on the magnitude and not on the direction of the applied field. More explicitly, for positive bias the most positive half of the square wave is expected to result in the maximum field, and for the negative bias the negative half gives the maximum field, hence producing the apparent phase reversal with respect to the phase reference, the fundamental ac component of the square wave. In this configuration, the phase lag between the fundamental harmonic of the observed signal $\Delta I/I$ and the fundamental harmonic of the applied square wave was 45° , which is relatively small and indicates that the waveform of the electric field is not too badly distorted from the square wave of the driving voltage.

The curves of Fig. 8 can be qualitatively explained as a composite of two phenomena: the electro-optic effect associated with the fundamental edge located at 0.42 eV ⁹ and the modulation of the optical properties of the Gouy layer of the electrolyte adjacent to the PbS film. The electro-optic effect appears as a dip around 0.4 eV in the broad curve of the electrolyte modulation. Modulation of the Gouy layer is apparently the cause of the structure observed by Feinleib in the electroreflectance of metals⁴⁴ and has been used to study the properties of semiconductor-electrolyte interfaces.⁴⁵ Use of the relatively high-resistivity electrolyte propylene carbonate with high-conductivity semiconductors is expected to enhance this effect, since more of the voltage drop will occur in the electrolyte.

⁴⁴ J. Feinleib, Phys. Rev. Letters **16**, 1200 (1966). See, however, A. Probst and W. N. Hanson, Phys. Rev. **160**, 600 (1967).

⁴⁵ W. N. Hansen, T. Kuwana, and R. A. Osteryoung, Anal. Chem. **38**, 1810 (1966).

Phenomenologically, the modulation of the electrolyte changes the optical matching between the PbS and the electrolyte and therefore changes the light transmitted through the film by a slight amount which varies in phase with the applied voltage. Calculation of the change depends upon a complicated but straightforward analysis of boundary conditions of plane waves at normal incidence passing through several layers of dielectric and possibly absorbing material. Since the dielectric constant of the hypothetical layer whose properties depend on the applied field is not known, a calculation of this effect was not attempted. Results to be presented for PbSe show the presence of interference modulation more clearly and we resume the discussion of this effect at that point.

The fact that the curves of the experimental results for the two bias conditions of Fig. 8 are nearly mirror images of each other suggests that there exists some dc bias condition for which a null signal could be obtained. This, however, cannot be done, as is shown in Fig. 9. The top two curves show the two dc biases which most nearly give a null signal for the sample of Fig. 8, one for 0.0 V and one for -0.1 V dc bias. These biases tend to equalize the Gouy layer contribution during each half-cycle, leaving what we take to be the electro-optic contribution to $\Delta I/I$ caused by the change of ϵ_2 in the film itself. Since the fundamental edge is a set of equivalent nearly spherically symmetric M_0 critical points located at the L points,¹² the electro-optic spectrum should be fitted by the function $F(\eta)$ if excitonic effects are neglected.²⁷ Keeping in mind the fact that the sign of $\Delta\epsilon_2$ is ambiguous for the maximum field condition, since the half of the square wave corresponding to maximum field is not known *a priori*, the

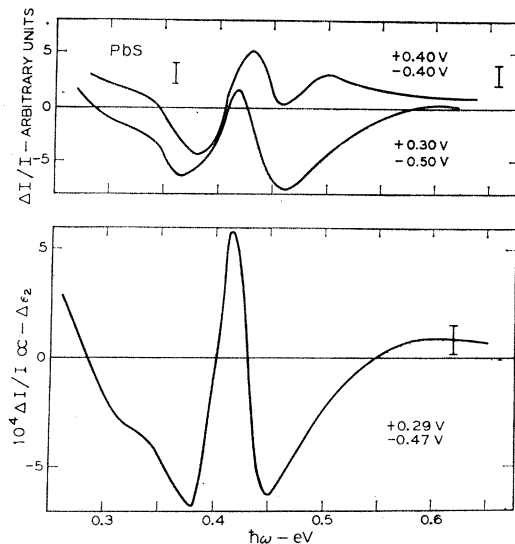


FIG. 9. Best null electroabsorption of PbS film of Fig. 8. The lower curve presents data for nearest-null signal taken by measuring ΔI and I separately and dividing. The upper two curves are to same scale as in Fig. 8.

zero dc bias curve could be approximated by a broadened $F(\eta)$ curve with a subsidiary oscillation. The curve taken with 0.0 V dc bias can be fitted to a certain extent by the broadened $-\Delta\epsilon_2$ curve given for the M_0 edge in Fig. 7 if one subsidiary oscillation is kept. The main peak should then be flanked by dips of equal depth in Fig. 9, but this does not occur. On the basis of Fig. 7, the energy gap should be at the zero crossing which is estimated as being between 0.40 and 0.41 eV.

The bias can be changed to make the dips of equal depth, as is shown by the remaining two curves of Fig. 9, but in so doing, the fit to the broadened $-\Delta\epsilon_2$ curve becomes worse. We obtain a shape which qualitatively resembles that of an exciton quenched in an electric field, characterized by a relatively large and sharp center spike flanked by two broad wings which has, for example, been seen in the electroabsorption spectra of Ge p - n junction diodes.⁴⁶ Because of the high dielectric constant of PbS, this exciton would occur at an energy nearly equal to that of the direct gap; we note that the dip in the curve in Fig. 9 occurs at the expected energy gap of 0.42 eV. The third curve in Fig. 9 shows an earlier measurement on the same sample at nearest-null conditions, obtained by making separate measurements of ΔI and I and dividing point by point. Since the half-width of the structure of the lower two curves is about $kT=0.026$ eV, this also suggests the excitonic electroabsorption effect. The measurements given by the lower and middle curve of Fig. 9 were taken two months apart (lower curve first), which gives some idea of the stability of the films in a dry atmosphere, but a somewhat overoptimistic view of the reproducibility of the electroabsorption data. A doped p -type epitaxial PbS film on NaCl gave similar results.

The equivalent electroabsorption spectrum for a nominal 0.5- μ PbSe epitaxial film deposited on a cleaved NaCl substrate is shown in Fig. 10. This PbSe film was p type and had the parameters $p=7\times 10^{18}$ cm⁻³, $\rho=0.016$ Ω cm, and $\mu_H=60$ cm² V⁻¹ sec⁻¹. Measurements were made with a cooled PbSe cell in order to provide detector sensitivity in an energy range below the room-temperature energy gap of PbSe, 0.27 eV.⁴⁷ Figure 10 gives the results of nearest-null signal bias and negative bias conditions. A curve for stronger positive bias was also taken, which was essentially the mirror image of the negative bias curve as in PbS, but is not shown. The negative bias curve consists primarily of oscillations resulting from interference in the PbSe film. This is clearly shown by the arrows which give the measured peak transmission (upward) and least transmission (downward) energies for the same film, measured on a Perkin-Elmer Model 337 dual beam spectrometer. The presence of a third transmission interference maximum is seen at about 0.58 eV.

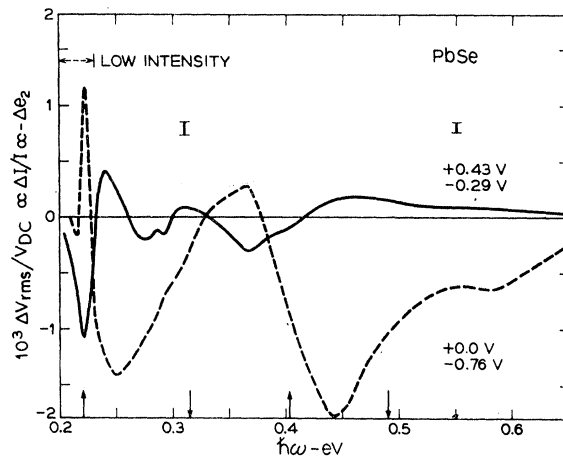


FIG. 10. Electroabsorption of nominal 0.5- μ p -type PbSe film epitaxially deposited on a cleaved NaCl substrate for best null and negative bias conditions. Arrows locate measured interference transmission maxima (\uparrow) and minima (\downarrow) in film.

The fact that the period of the interference oscillations fits so well the observed gross structure in the electroabsorption oscillations demonstrates the dependence of the latter on the former. We have observed identical phenomena in GeTe and SnTe thin films, which persist for several tenths of an eV above the onset of the absorption edge and remain visible well after the same interference pattern has vanished in transmission. Under sufficiently high resolution, interference oscillations associated with the electrolyte film can also appear and have been observed.

Structure in Fig. 10 below 0.24 eV is measured at very low light intensities due to CO₂ absorption and equipment limitations and should not be taken as an effect in the crystal itself, but is rather probably due to a slight offsetting of the reference channel zero which can cause large errors at very low light intensities. It should be pointed out that the intensities over the remainder of the spectrum were sufficiently large to prevent errors of this sort, and in particular the image of the transmission interference in the $\Delta I/I$ spectrum is caused by the interference modulation referred to earlier and not to a change in I .

In further support of electroabsorption oscillations produced by interference oscillations we show electroabsorption results for a thinner PbSe epitaxial film on a NaCl substrate in Fig. 11. This film was of nominal 0.4 μ thickness, with $p=4\times 10^{18}$ cm⁻³, $\rho=0.016$ Ω cm, and $\mu_H=110$ cm² V⁻¹ sec⁻¹. The spectrum is quite different from that of Fig. 10 from the standpoint of interference oscillations in the PbSe film. The notch at 0.36 eV in the two large curves is again the result of a slightly incorrect zero adjustment in the reference or I channel and represents division by "zero" at the point where C—H bonds of the electrolyte lead to particularly strong absorption (3.4 μ). This error is negligible elsewhere, and except for the extremely low light intensities

⁴⁶ Y. Hamakawa, F. Germano, and P. Handler, in *Proceedings of the International Conference on the Physics of Semiconductors* (The Physical Society of Japan, Tokyo, 1966), p. 111.

⁴⁷ A. J. Strauss, *Phys. Rev.* **157**, 608 (1967).

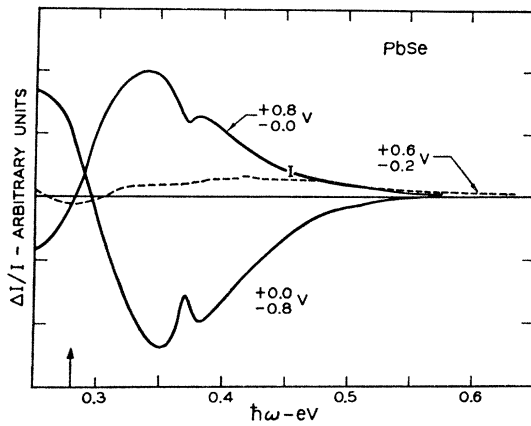


FIG. 11. Electroabsorption of nominal $0.4\text{-}\mu$ p -type PbSe film epitaxially deposited on a cleaved NaCl substrate for best null and large bias conditions. Arrow indicates transmission maximum of film.

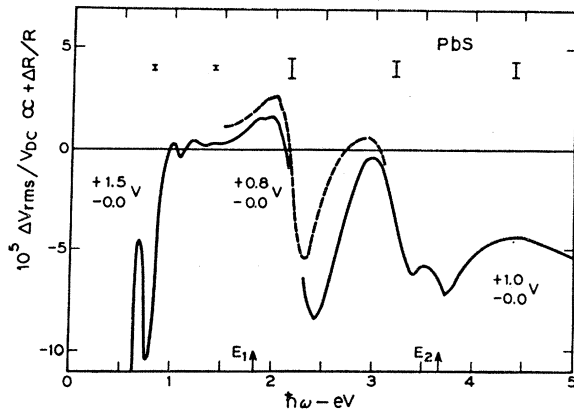


FIG. 12. Electroreflectance of PbS film of Fig. 8 for various positive biases. PbS, infrared phototube, and uv phototube detectors are used in their optimum energy regions. Error bars refer to appropriate uncertainties. Arrows indicate respective structures in reflectance.

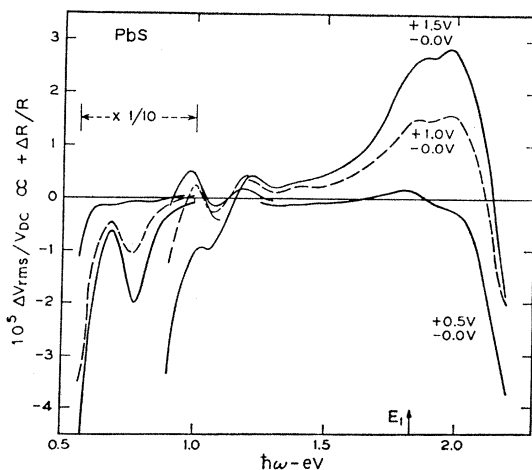


FIG. 13. Electroreflectance of PbS film of Fig. 8 below 2.2 eV for various conditions of bias and square-wave amplitude. Note scale change below 1 eV .

encountered below 0.24 eV using the cooled PbSe detector, appears nowhere else in electroabsorption measurements. The notch is missing in the nearest-null bias curve.

Since PbSe has essentially the same direct-gap band structure as PbS, namely, four equivalent spherically symmetric M_0 critical points at the L points of the Brillouin zone at a room-temperature threshold of 0.27 eV , the electroabsorption spectra for the nearest-null bias condition, where the electro-optic effect dominates, should be quite similar to that of PbS. Some structure is observable near the energy of the direct gap in both Figs. 10 and 11, but is too poorly resolved to relate to any electro-optic structure. This may be due to the higher carrier concentration of the PbSe films with respect to the PbS film measured earlier, which would broaden exciton absorption and tend to lower the internal field in the semiconductor by dropping a greater fraction of the voltage in the electrolyte.

We next consider the electroreflectance results for PbS and PbSe. Figures 12 and 13 give typical electroreflectance spectra for the same PbS film used in electroabsorption measurements for a range of bias and square-wave amplitudes. The phase lag between the fundamental harmonics of the 100-Hz square wave and the resultant change of intensity was 135° , which means that the internal field was considerably distorted from the driving voltage. For this reason we give as ordinate variable the ratio of rms change in detector voltage caused by ΔI to the dc value of the voltage for phototubes, or shift from dark voltage for PbS or PbSe detectors, which is proportional to I . This ratio is proportional to $+\Delta R/R$. Because neither the time variation of ΔI nor the internal field is known, the amplitude of the fundamental harmonic of ΔI cannot be related to a change of intensity resulting from a given internal field and therefore the constant relating $\Delta R/R$ with the output voltage cannot be determined. No information is therefore lost by using $\Delta V_{\text{rms}}/V_{\text{dc}}$ as the ordinate.

PbS, infrared phototube, and uv phototube detectors are used in their optimum regions and the overlap regions indicate the usual reproducibility. Spectra taken with the infrared phototube are shown as dotted lines in Fig. 12 in order to distinguish among the three types of detectors. For comparison purposes we give the electroreflectance spectra of a thick natural PbS crystal in Figs. 14 and 15. The cell phase lag for this crystal was 70° , compared to 135° in the thin films, indicating a sizeable phase shift in the thin film is occurring because of its higher resistance. Figures 13 and 14 show curves taken at several different biases and square-wave amplitudes in order to illustrate some of the changes in the spectra which result from changing the voltage. As a general rule we give the spectra corresponding to maximum voltage, since the structure for these voltages was most pronounced. The location of the peaks in the structure is fairly insensitive to variations of driving

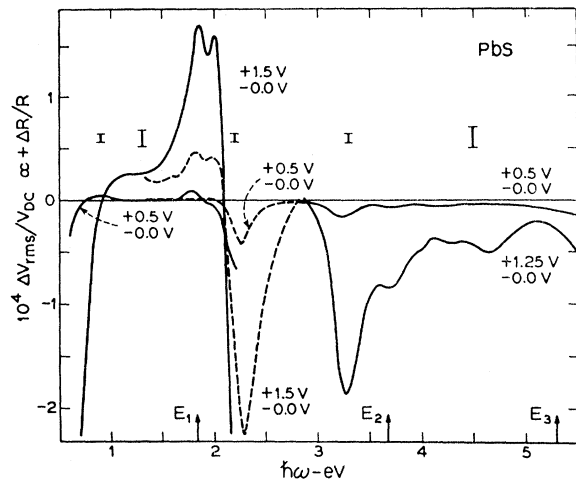


FIG. 14. Electroreflectance of thick natural crystal of PbS for several conditions of positive bias. Uncertainties are indicated by error bars. Reflectivity structure is located by arrows.

voltage of a given polarity, but depends somewhat on the polarity. Positive bias results are generally more consistent and we base the analysis primarily on these. Although more structure appears with higher voltages, the onset of electrochemical reactions imposes an upper limit. These reactions generally occurred if the applied potentials exceeded 1.5 V of either polarity for the frequencies used, and were enhanced by shining light on the interface. A tarnishing of the surface and subsequent destruction of the film followed.

Similar results for the 0.4- μ PbSe film used in electro-absorption are presented in Figs. 16 (the lower set of curves) and 17. Figure 17 shows a set of positive bias measurements for this film which show the change of peaks with bias and signal amplitude in the region below 2 eV. For comparison, we present in the upper set of curves of Fig. 16 the equivalent electroreflectance spectrum of a PbSe film deposited on a cleaved mica substrate, with nominal thickness 0.5 μ , $p=9 \times 10^{18}$

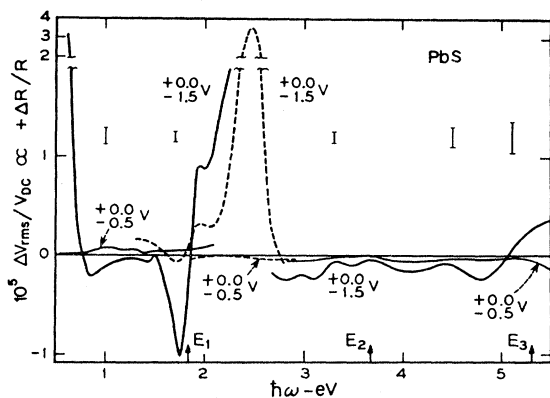


FIG. 15. Electroreflectance of PbS crystal of Fig. 14 for negative bias. Note ordinate scale change.

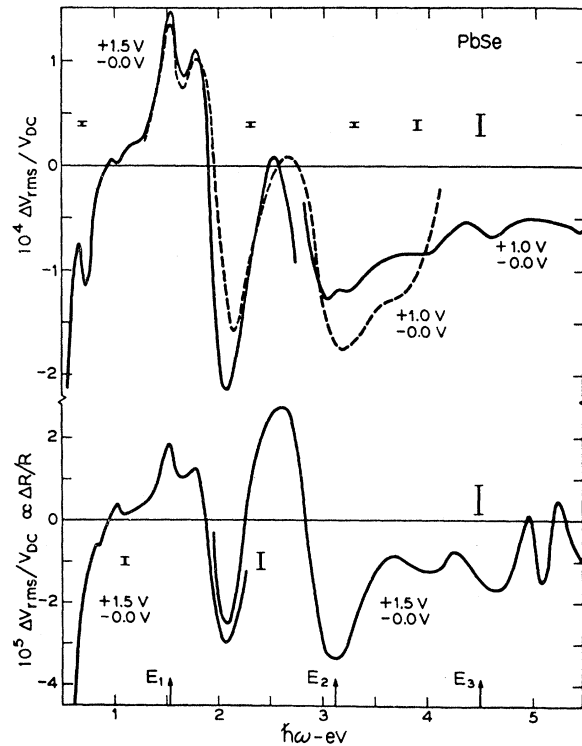


FIG. 16. The upper set of curves shows electroreflectance of nominal 0.5- μ *p*-type PbSe film deposited on cleaved mica substrate, for positive bias. The lower set gives the electroreflectance spectrum of the PbSe film of Fig. 11 (NaCl substrate) under similar conditions.

cm^{-3} , $\rho=0.011 \Omega \text{ cm}$, and $\mu_H=60 \text{ cm}^2 \text{ V}^{-1} \text{ sec}^{-1}$. The use of mica as a substrate resulted in a more durable film.

Comparison of the electroreflectance results for PbS and PbSe, as, for example, Figs. 12-14 with Figs. 16 and 17, shows the similarity between the two compounds, which is expected from the nearly identical band structures and the similarity of their reflectance curves given in Fig. 5. The energies of the various structures in the reflectance curves, namely, the E_1 structure at 1.83 eV (1.54 eV), the E_2 or reflectivity maximum at 3.6 eV (3.1 eV), and the shoulder at E_3 of energy 5.3 eV (4.5 eV) in PbS (PbSe), are indicated on Figs. 12-17 by arrows at the appropriate energies. We expect structure in the electroreflectance spectra to correlate with the structure in reflectance, and find to a certain extent that this is indeed the case.

Structure which occurs in both PbS and PbSe below 1.2 eV is due to optical matching of the electrolyte in the back-reflected signal similar to that seen in electro-absorption and is not due to critical-point structure in the crystals themselves. This is seen immediately by comparing the epitaxial film results of Fig. 12 for PbS with that of the thick natural crystal given in Figs. 14 and 15. The interference vanishes when the optical density of the film becomes sufficient to cut off the back-

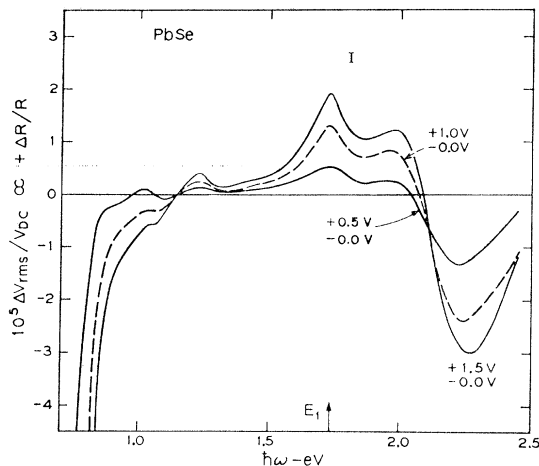


FIG. 17. Electroreflectance of PbSe film of Fig. 11 below 2.3 eV for various bias conditions.

reflected light component. The off-scale travel of the electroreflectance signal in all curves at 0.6 eV is due to the onset of absorption in the electrolyte and is not produced by the band structure of the epitaxial films, as can be seen by the complete lack of electroabsorption structure in this region in Figs. 8 and 9, from the absence of any transitions in the energy range from the band-structure calculations, and from the fact that the structure occurs at the same energy for each material (PbTe included).

In contrast to the electroabsorption measurements, considerable distortion of the resulting internal field from the applied voltage square wave was present in electroreflectance as evidenced by the large phase lag, which has been discussed in connection with the use of $\Delta V_{rms}/V_{dc}$ as the ordinate variable. This distortion also affects the electro-optic function shape, particularly in the subsidiary oscillations, since it averages over a range of fields per cycle of driving voltage. This can be seen as follows. The measuring system takes the first Fourier component of the relatively complicated periodic function $\Delta I(t)$, which consists of a broadened electro-optic function combination for a range of fields. Since the primary effect of the field is to change the period of oscillations in energy of the electro-optic functions, which varies as $\hbar\theta = (e^2 \mathcal{E}^2 / 2\mu\hbar)^{1/3}$, the subsidiary oscillations for photon energies off threshold will tend to average each other out; since the functions all add in phase at photon energy equal to threshold, electro-optic structure will tend to be unaffected at this energy. This leads to a relative enhancement of electro-optic structure at the threshold energy itself. Spatial variation of the electric field within the film further increases this effect. For this reason we assume that all electroreflectance structure occurs at the threshold of the critical point, and that the only legitimate shape analysis is that of the sign of the change of reflected intensity with field. This sign can be related

to possible critical points through Figs. 6 and 7. The spatial and time averages will further modify the broadened F function shown (i.e., $\Delta\epsilon_2$ for the M_0 edge) so as to suppress the subsidiary oscillation, which cuts into the peak just above threshold (for M_0) and weakens it considerably. The dominant peak in this function thus tends to be that arising from the sharp peak at threshold in the unbroadened F function²⁷; hence we consider structure arising from broadened F functions to have the sign of this peak.

In the analysis of the electroreflectance spectrum of PbS and PbSe we consider first the structure which occurs at 2.3 to 2.4 eV in PbS and 2.05 eV in PbSe and which dominates the spectrum in Figs. 12–17 (except Fig. 13, where it occurs beyond the energy range). Since its peak energy position is reasonably independent of the bias, it seems logical to assume that this peak represents a critical point and is not a subsidiary oscillation of a critical point several tenths of an eV away. In any event such a subsidiary oscillation would be expected to have a much smaller amplitude than the main peak due to space and time averaging as discussed earlier. Since the inversion of the sign of the peak with changing dc bias (compare Fig. 14 with Fig. 15) shows that the nonzero half of the square wave represents the maximum field condition, we look for a critical point such that the reflectance decreases at its threshold energy with the application of an electric field, because $\Delta R/R$ is out of phase with the ac component of the applied voltage for positive bias. At 2.3 eV for PbS, Fig. 6 shows $\Delta R/R$ is proportional to $+\Delta\epsilon_2$. The proper negative sign at the critical point for the observed change in reflectivity is obtained only with M_1 or M_2 transitions, either for electric field parallel or transverse to the axis of mass of odd sign, as Fig. 7 shows. The same considerations apply to PbSe.

No M_2 transition appears in this energy region for either PbS or PbSe, although several M_1 transitions are present. A particular M_1 transition which may have a sufficiently large effect to show up strongly in the electroreflectance spectrum is the $\Sigma_1^5(3) \rightarrow \Sigma_1^5(2)$ transition 0.58 of the way from Γ to K in Fig. 2 which has a threshold energy of 2.5 eV in PbS. Continuing along Σ , we find that the band separations at Γ and K are 6.6 and 6.0, respectively, suggesting a fairly small positive mass in the Σ direction. In the two perpendicular directions, there is first the intersection with Δ , 0.87 of the distance from Γ to X ; the energy separation here is about 7.0 eV by Fig. 2, which again is likely to lead to a small positive mass toward Δ . The remaining direction perpendicular to both Σ and $\Sigma \rightarrow \Delta$ intersects Λ 0.87 from Γ to L . Here the energy separation of 2.0 eV leads to a fairly large negative mass. Assuming monotonic variation of E with \mathbf{k} in these directions, the $\Sigma_1^5(3) \rightarrow \Sigma_4^5(2)$ transition is therefore an M_1 transition with a [100] negative mass appreciably larger than that of the two positive masses in the perpendicular directions. Assuming a reasonable matrix element, the

statistical weight of eight critical points transverse to the [100] field, in combination with the large negative mass which increases the density of states, should result in a contribution to the electroreflectance spectrum. The remaining Σ transitions, $\Sigma_1^5(3) \rightarrow \Sigma_1^5(4)$ at 1.5 eV, $\Sigma_4^5(1) \rightarrow \Sigma_1^5(4)$ at 2.85 eV, and $\Sigma_6^5(1) \rightarrow \Sigma_1^5(4)$ and $\Sigma_4^5(1) \rightarrow \Sigma_4^5(2)$ at 3.9 eV, apparently do not have such a large negative mass or matrix element and therefore may not contribute. This assignment should be checked by an estimation of the matrix elements of the transitions in the Σ direction, and also by obtaining the location of the corresponding Σ transitions in PbSe from band-structure calculations when the necessary calculations become available. On the basis of the present status of theory and experiment, it appears that the transition given is responsible for this dominant peak.

The first electroreflectance structure occurs just below this main peak, and consists of two peaks located at 1.85 and 1.98 eV in PbS, and 1.53 and 1.78 eV in PbSe, as shown most clearly in Figs. 13 and 17. The lower energy structure of the pair coincides with, and therefore must be, the same transition(s) that results in the E_1 shoulder in reflectance. The type of critical point involved can be determined with the help of Fig. 6, which shows that the electroreflectance spectrum at these energies also comes from $+\Delta\epsilon_2$. Since ΔI and the applied voltage are in phase for positive bias, the reflectivity and therefore ϵ_2 must increase with increasing field because the maximum field is associated with the positive half of the square wave for positive bias. Figure 7 shows this behavior is characteristic of an M_0 threshold and opposite that of an M_1 , for either parallel or transverse field orientation. On this basis the structures are assigned to M_0 transitions.

Barring critical points at general points in the zone, there are four possible M_0 or M_0 -like transitions at L , by Table I, which are close enough in energy to cause this structure. Although the transitions $L_3^{45}(1) \rightarrow L_{2,6'}(2)$ and $L_3^6(1) \rightarrow L_{2,6'}(2)$ may be M_1 at the point L itself, the band structure shows that they are located very near the minimum energy separation which apparently occurs just off L along Δ , and therefore would be expected to have some M_0 -type structure associated with them at slightly lower energy. These M_0 critical points should be separated by approximately the same splitting as the bands at L .

The transition $L_1^6(2) \rightarrow L_3^{45'}(1)$ at 2.25 eV in PbS and 2.00 eV in PbSe can be eliminated because it would make the PbS peak separation greater than the PbSe separation for any of the remaining M_0 transitions, since it can be safely assumed that both peaks arise from the same transitions in each compound. If only one of the $L_3^{45}(1)$, $L_3^6(1) \rightarrow L_{2,6'}(2)$ transitions were chosen, the question of why the matrix element of the other should be so much less, since they arise from the doubly degenerate L_3 representation in the absence of spin-orbit splitting, would have to be answered. How-

ever, it should be noted that the calculated spin-orbit splittings of 0.08 and 0.15 eV are less than the measured separations of 0.13 and 0.25 eV for PbS and PbSe, respectively; this discrepancy is probably not serious and in any event the correct greater separation for PbSe is obtained. Assuming that for some reason the $L_3^6(1)$ transition were not visible, no better agreement would result by assigning the remaining transition $L_1^6(2) \rightarrow L_{3,6'}(1)$ to the lower peak and $L_3^{45}(1) \rightarrow L_{2,6'}(2)$ to the upper peak, for then the separations would be 0.20 and 0.37 eV, respectively. Considering that the two transitions $L_3^{45}(1) \rightarrow L_{2,6'}(2)$ and $L_3^6(1) \rightarrow L_{2,6'}(2)$ should be of roughly equal strength and behavior, these must be considered as the transitions responsible for the 1.85- and 1.98-eV peaks in PbS, and the 1.53- and 1.78-eV peaks in PbSe. The E_1 reflectivity structure therefore must arise from the transition $L_3^{45}(1) \rightarrow L_{2,6'}(2)$ in PbS and PbSe, and the spin-orbit splittings at L between $L_3^6(1)$ and $L_3^{45}(1)$ are 0.13 and 0.25 eV in PbS and PbSe, respectively.

At higher energies Fig. 6 shows that the electroreflectance spectrum is given essentially by $\Delta R \propto -\Delta\epsilon_1$ in the range of 3 to 4 eV in PbS and from 2.4 to 2.8 eV in PbSe. Beyond these energies, we have approximately

$$\Delta R \propto -\Delta\epsilon_1 - \frac{1}{2}\Delta\epsilon_2$$

for PbS, and

$$\Delta R \propto -\Delta\epsilon_1 - \Delta\epsilon_2$$

for PbSe.⁴⁸ Since all peaks in these energy ranges appear as intensity decreases with positive bias at maximum field, the structures responsible must have $\Delta\epsilon_1 > 0$, and probably have $\Delta\epsilon_2 > 0$, upon the application of a field. These inequalities are satisfied at the critical-point energy only by the M_2 critical point for $\Delta\epsilon_1$, in both parallel and transverse field orientations, and by the M_0 or M_3 edges if $\Delta\epsilon_2$ is observable. Since we expect $\Delta\epsilon_1$ to dominate in these regions, structure above 3 eV is apparently caused by M_2 critical points most probably located along Δ or at X . Accordingly, we can make the following (speculative) identifications. The large peak at 3.3 eV in PbS and 3.0 eV in PbSe is probably $\Delta^6(4) \rightarrow \Delta^6(5)$, occurring at 3.0 and 2.8 eV in PbS and PbSe, respectively; 3.7 and 3.3 eV from $\Delta^7(1) \rightarrow \Delta^6(5)$ at 4.0 and 3.8 eV; 4.0 and 3.8 eV from $\Delta^6(3) \rightarrow \Delta^6(5)$ at 4.1 and 3.9 eV; 4.6 and 4.6 eV from $\Delta^6(4) \rightarrow \Delta^6(6)$ at 4.4 and 4.6 eV, respectively. This by no means exhausts the critical points available to be fitted and should not be taken as a final description of the high-energy electroreflectance structure, since the electroreflectance signals are too broad to be interpreted uniquely as being due to transitions of the M_2 type. The electroreflectance technique enhances the structure but reaches its limitation in PbS and PbSe at these energies with respect to detailed interpretation of the critical-point structure.

⁴⁸ The difference between these expressions of ΔR for PbS and PbSe may not be real, but may be produced by inaccuracy in the Kramers-Kronig analysis of R used to obtain α and β .

B. PbTe

Due to the larger spin-orbit splitting of Te, the band structure of PbTe, as calculated by Lin and Kleinman and given in Fig. 4, is somewhat different from that of PbS and PbSe. The column of energies for PbTe in Table I, obtained from Fig. 4, shows that the critical points are ordered quite differently in energy, with the major changes occurring in the Brillouin zone region about the fundamental energy gap where the $L_{2,6'}$ (2) conduction band of PbS and PbSe has been inverted with the band $L_{3,6'}$ (1). One effect of this is to make the M_0 critical points of the fundamental threshold highly anisotropic.^{12,23} In spite of these changes, the reflectivity spectrum of PbTe is quite similar to that of PbS and PbSe except for being shifted to lower energy, as seen in Fig. 5. The dominant reflectivity features in the range of interest here are the E_1 shoulder at 1.25 eV, the E_2 reflectivity peak at 2.3 eV, and the E_3 shoulder at 3.5 eV.

We consider first the electroabsorption measurements. Figure 18 shows the electroabsorption spectrum of a nominal $0.5\text{-}\mu$ p -type epitaxial PbTe film of resistivity $0.044\ \Omega\ \text{cm}$, $p=7\times 10^{17}\ \text{cm}^{-3}$, and $\mu_H=260\ \text{cm}^2\ \text{V}^{-1}\ \text{sec}^{-1}$, deposited in the usual manner on a cleaved NaCl substrate. In this material the spectrum is quite similar to that of PbS and PbSe. The electroabsorption structure can be obtained from the condition of best null. The gap measured in Fig. 18 is 0.30 eV from the best null curve. The energy gap for PbTe at room temperature as determined by resistivity and Hall-effect measurements is known to be 0.32 eV.^{4,5} The difference is probably due to a certain amount of strain present in the film, since this crystal rapidly developed a crazed appearance following measurement and disintegrated soon afterward. The indirect valence-conduction band transition at 0.36 eV^{4,5} may be contributing some structure at this energy but the structure present does not constitute a demonstration of this

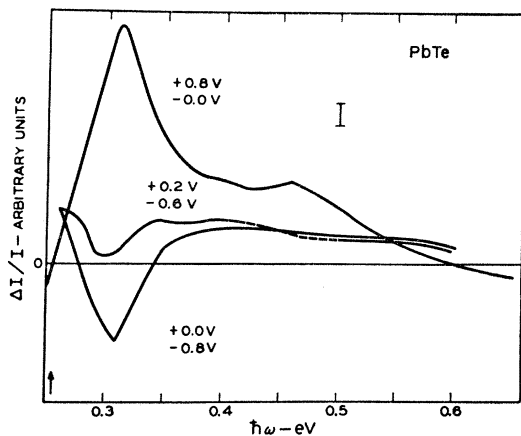


FIG. 18. Electroabsorption of nominal $0.5\text{-}\mu$ p -type epitaxial PbTe film on NaCl substrate, for various conditions of bias. Arrow locates measured interference transmission maximum.

transition. Further measurements are being planned in an attempt to observe this transition.

Because of the greater durability of the PbTe films epitaxially deposited on mica, the reflectivity measurements were carried out on a film of PbTe nominally $0.5\ \mu$ thick deposited on this substrate. This film had the properties $p=1.2\times 10^{18}\ \text{cm}^{-3}$, $\rho=0.040\ \Omega\ \text{cm}$, and $\mu_H=130\ \text{cm}^2\ \text{V}^{-1}\ \text{sec}^{-1}$. Results of electroreflectance measurements on this film from 0.6 to 5 eV are shown in Figs. 19 and 20. The usual epitaxial film interference oscillations appear below 0.8 eV until the optical density is sufficient to inhibit back-reflection effects. The inversion of the electroreflectance signal with dc bias

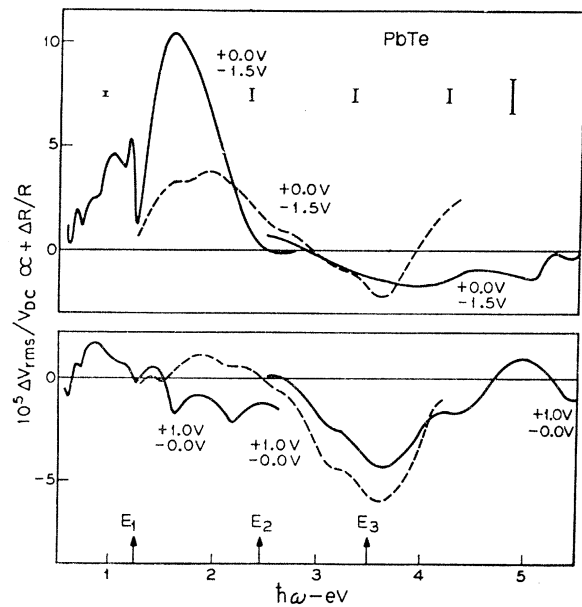


FIG. 19. The upper set of curves show electroreflectance of nominal $0.5\text{-}\mu$ p -type PbTe film deposited on mica substrate, for negative bias. The lower set of curves give electroreflectance of same film for positive bias. Arrows locate structure in reflectivity. PbS, infrared phototube, and uv phototube detectors are used in their optimum regions, with uncertainties shown.

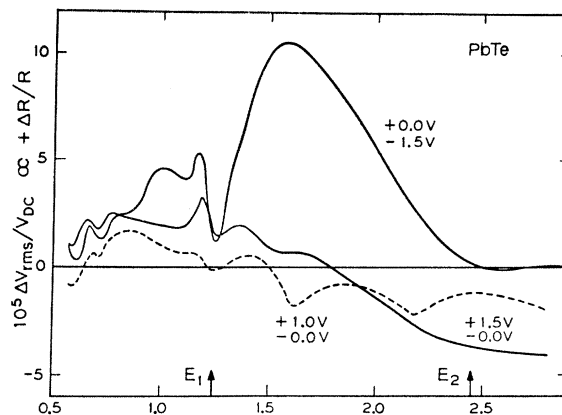


FIG. 20. Electroreflectance of PbTe film of Fig. 19 in energy region below 2.5 eV for various bias conditions.

which occurred for PbS and PbSe is absent in PbTe, shown by comparing the upper and lower sets of curves in Fig. 19. This indicates that surface shielding is passing only the ac component of the applied voltage. With effectively no dc, equal fields (of opposite sign) should presumably result from the applied square wave voltage. This means that the maximum-field half of the square wave is not directly obtainable, in contrast with PbS and PbSe. This absence of phase reversal indicates as well that what is seen in electroreflectance is an electro-optic effect and probably not an effect associated with the Gouy layer, since the Gouy layer caused interference oscillations seen in electroabsorption in Fig. 18 inverted sign with an inversion of dc bias.

The band structure of Fig. 4 indicates that of the transitions at L , only those arising from $L_1^6(2)$, the upper valence band, will be of the type M_0 . The remaining will be relatively complicated, probably being M_1 at L , but since the bands reach their minimum separation very near L , will have a very close M_0 transition, lying along Λ , associated with them. All transitions at L occur at energies below 3 eV; hence any structure at higher energies must involve Δ , Σ , X , Λ , or some arbitrary point of the zone.

The first electroreflectance structure beyond the band edge is seen most clearly in Fig. 20 and appears from 1.18 to 1.25 eV, coming out quite rapidly with higher applied voltage as is to be expected from an electro-optic effect. The width of the structure, about 100 meV, is also consistent with the electro-optic interpretation. In fact, of all electroreflectance structures observed in the lead salts, this is the only one which appears to be a clear-cut electro-optic effect. Of the several possible transitions listed in Table I and 1.2 eV for PbTe, the most reasonable appears to be the $\Sigma_1^5(3) \rightarrow \Sigma_4^5(2)$ transition at 1.15 eV. This transition is of the M_1 type with a negative mass somewhat larger than the two transverse positive masses and lying along the (100) perpendicular from Σ which intersects Λ . Therefore, the electro-optic spectrum should result from 12 essentially transverse-type M_1 spectra since the field probably lies in the (111) direction.³⁶ Even for random orientations of PbTe, the small transverse masses would dominate the large longitudinal negative mass and cause a predominantly, if not completely, transverse electroreflectance spectrum. In any event only the transverse M_1 spectrum should appear.

The half of the square wave which results in the largest field can be deduced from the change in the peak magnitude even though the dc bias is almost completely blocked by interface effects. We note from Fig. 20 that the signal is greatest for a 1.5 V amplitude square wave with -0.75 V dc bias, and conclude that the negative swing of the square wave, where the electrolyte is positive with respect to the crystal, results in the highest field. Therefore, since intensity change and square wave are in phase for the lower

energy and out of phase for the higher energy part of the electroreflectance structure, we look for $\Delta\epsilon_1$ and $\Delta\epsilon_2$ such that ΔR decreases with field at lower energies and increases at higher energy. Figure 6 shows that to a good approximation only $+\Delta\epsilon_2$ will contribute to $\Delta R/R$ for PbTe in contact with a $n=1.400$ electrolyte at this energy. Figure 7 shows that the particular variation observed in Fig. 20 is opposite to that of the M_0 and M_1 parallel electro-optic effect, but correct for an M_1 transverse effect. Since the energy is reasonably close as well, it appears that the structure is due to the $\Sigma_1^5(3) \rightarrow \Sigma_4^5(2)$ transition. The alternate choice of the $L_3^6(1) \rightarrow L_3^{6'}(1)$ M_0+M_1 complex can probably be eliminated because it occurs at too high an energy and may have appreciable M_0 behavior. The remaining possible transitions are all M_0 and can be eliminated.

This transition is also responsible for the E_1 structure in reflectance since it occurs at precisely the same energy. We here disagree with LK, as they assign the M_0 transition $L_1^6(2) \rightarrow L_2^{6'}(2)$ to the E_1 reflectivity structure. This occurs quite close in energy as well but the electroreflectance spectrum observed is that of an M_1 structure and not M_0 , which eliminates the L transition as the cause of the E_1 shoulder. We note that the structure at 1 eV appearing in the large negative bias curve of Fig. 20 can only come from the M_0+M_1 complex of $L_3^{45}(1) \rightarrow L_3^{6'}(1)$ at 0.98 eV in Table I, from the sign of the structure and lack of other transitions which could give M_1 -like behavior.

To obtain the type of critical point associated with the large peak at 1.6 eV, we note from Fig. 6 that $\Delta R/R$ is given by almost equal contributions of $-\Delta\epsilon_1$ and $+\Delta\epsilon_2$ at this energy. The decrease of reflectance with field observed in Figs. 19 and 20 therefore requires a critical point satisfying $\Delta\epsilon_1 >$ and $\Delta\epsilon_2 < 0$. But this can only come from an M_2 critical point; either parallel or transverse field orientation is permitted. The M_1 critical point can be eliminated by the equal contribution of $-\Delta\epsilon_1$ and $+\Delta\epsilon_2$ given in Fig. 6, since for this threshold $\Delta\epsilon_1$ and $\Delta\epsilon_2$ are approximately equal, are of the same sign, and would therefore tend to cancel each other. The only possible M_2 transition listed in Table I is the lowest-energy one, that of the $\Delta^6(4) \rightarrow \Delta^6(5)$ transition at 1.8 eV. This is quite close to the value of 1.6 eV observed for this structure, and it therefore appears that this is the critical point responsible for the transition.

The next structure, which appears most strongly in the positive bias curve of square-wave amplitude 1.0 V in Fig. 20, occurs at 2.2 eV and is also of negative $\Delta R/R$. Figure 6 gives the major contribution as that of $-\Delta\epsilon_1$ for this peak, which requires a critical point producing $\Delta\epsilon_1 > 0$. Once again the only possible choice is an M_2 critical point. Once this has been determined, the only possible M_2 transition along a high-symmetry direction is the $\Delta^7(1) \rightarrow \Delta^6(5)$ transition at 2.6 eV. The 0.4-eV discrepancy seems rather large, yet on the basis of the assumptions going into the analysis the M_2 nature of

the critical point follows unambiguously, which eliminates all remaining transitions in the energy range.

One of the curious features of PbTe is the almost complete lack of electroreflectance structure in the region of the E_2 reflectivity peak at 2.4 eV. Pronounced structure corresponding to the E_3 shoulder is observable at 3.5 eV, but the E_2 peak apparently yields nothing but an inflection point in the electroreflectance spectrum. This behavior is conceivable for a self-cancellation of the electroreflectance spectrum between $\Delta\epsilon_1$ and $\Delta\epsilon_2$, which contribute approximately as $\Delta R/R \propto -\Delta\epsilon_1 - \frac{1}{2}\Delta\epsilon_2$. An M_0 threshold, where $\Delta\epsilon_1$ and $\Delta\epsilon_2$ are of opposite sign, could possibly produce this behavior. It may be possible for the $L_3^6(1) \rightarrow L_{2,\delta'}(2)$ complex at 2.5 eV assigned by LK to this peak to provide this cancellation, although it is also conceivable that the electro-optic spectrum of this peak is too small because of large masses in all directions.

We conclude by noting that on the basis of the sign of $\Delta R/R$ at the E_3 peak in Fig. 19, this structure is consistent with M_1 transitions but probably not M_2 transitions, since $\Delta R/R \propto -\Delta\epsilon_1 - \frac{1}{2}\Delta\epsilon_2 > 0$ if we interpret the structure on the basis of the electro-optic effect. Remaining structure is too vague for a definite assignment. Strain measurements may yield more information about these peaks and lead at least to a narrowing of the choices available.

V. CONCLUSION

We have measured the electro-optic effect in PbS, PbSe, and PbTe in electroreflectance over the range of 0.6 to 5.5 eV, and electroabsorption from 0.25 to 0.65

eV, on an assortment of epitaxially deposited films and one natural crystal of PbS. Strong enhancement of the reflectivity spectrum was obtained, as expected with the electro-optic effect, and in addition peaks appeared which had no observable correlation with the reflectance spectrum. These structures have been related to critical points in the band structure calculated by Lin and Kleinman,²² and in general support the theoretical calculations. It was not possible to make unique identifications of the critical points in the optical spectrum in most of the energy range over 2.5 eV, a shortcoming which may be resolved by the use of strain measurements in conjunction with the electroreflectance results.

The use of a conducting transparent window in the infrared for electroabsorption measurements permitted measurements to be made in an energy region where the electrolyte was absorbing, and yielded structure in PbS which under certain bias conditions appeared excitonic rather than looking like the theoretical electro-optic curves calculated on the basis of no Coulomb interaction. This method should have general applications for electro-optic measurements in other low-gap semiconductors with energy gaps in regions where the usual electrolytes absorb strongly.³⁹

Interpretation of the results could be placed on a firmer basis (or shown to be incorrect) if the transition probabilities for the various critical points could be obtained. Certain structures, such as the twin-peaked structure occurring below 2 eV in PbS and PbSe, could be unambiguously determined if this information were available. Strain measurement will also yield more information about these critical points.